UNCLASSIFIED

Defense Technical Information Center
Compilation Part Notice

ADP010643

TITLE: Rotorcraft Damage Tolerance Evaluated by Computational Simulation

DISTRIBUTION: Approved for public release, distribution unlimited

This paper is part of the following report:

TITLE: Application of Damage Tolerance Principles for Improved Airworthiness of Rotorcraft [l'Application des principes de la tolerance a l'endommagement pour une meilleure aptitude au vol des aeronefs a voilure tournante]

To order the complete compilation report, use: ADA389234

The component part is provided here to allow users access to individually authored sections of proceedings, annals, symposia, ect. However, the component should be considered within the context of the overall compilation report and not as a stand-alone technical report.

The following component part numbers comprise the compilation report:

ADP010634 thru ADP010648

UNCLASSIFIED

Rotorcraft Damage Tolerance Evaluated by Computational Simulation

Christos C. Chamis*
National Aeronautics and Space Administration
Lewis Research Center, Cleveland, Ohio 44135-3191

Levon Minnetyan
Clarkson University, Potsdam, New York 13699-5710

Frank Abdi
AlphaStar Corporation, Long Beach, CA 90804

ABSTRACT

An integrally stiffened graphite/epoxy composite rotorcraft structure is evaluated via computational simulation. A computer code that scales up constituent micromechanics level material properties to the structure level and accounts for all possible failure modes is used for the simulation of composite degradation under loading. Damage initiation, growth, accumulation, and propagation to fracture are included in the simulation. Design implications with regard to defect and damage tolerance of integrally stiffened composite structures are examined. A procedure is outlined regarding the use of this type of information for setting quality acceptance criteria, design allowables, damage tolerance, and retirement-for-cause criteria.

KEYWORDS: Composites, Composite Shells, Composite Structures, Computational Simulation, Damage, Degradation, Durability, Fracture, Integrated Stiffening, Laminates, Structural Degradation.

INTRODUCTION

Laminated composite structures are used in many aerospace applications such as rotorcraft components, advanced aircraft fuselage, rocket motor cases, pressure vessels, containment structures, and other components with various shapes and sizes. In these applications composite structures are required to withstand significant in-plane loads. Additionally, composite structures are required to possess sufficient bending stiffness to resist buckling. Discussion in the current paper is focussed on integrally stiffened composite structures subjected to in-plane loads and internal/external pressures. Damage initiation, growth, accumulation, and propagation to fracture is simulated for composite panels and cylindrical shells with and without integrated stiffening layups. The influence of integrated stiffeners is examined with regard to out of plane stiffness contribution as well as damage progression and structural durability assessment under applied loading. Changes in the damage initiation load and the structural fracture load are quantified due to the presence of integrated stiffeners.

Integrally stiffened composite structures are manufactured by adding additional plies or braids that are designed to improve both the out-of-plane stiffness and buckling resistance of composite structural components. Integrated stiffening is typically obtained within the manufacturing process of a composite material. The layup of a laminated composite or the braid structure of a braided composite may be spatially concentrated to obtain a stiffening of the composite in the desired orientations. Integrally stiffened composites would display logical patterns of ply/braid concentrations. For example, a rectangular composite panel may be stiffened by adding bands of layers with fibers along the diagonals of the panel. Another example is the superposition of lattice type periodic angled stiffeners over a smooth composite plate layup during the manufacturing process. Integrated stiffening of composites may be obtained by hand layup of composite tape, filament winding, or by automated braiding processes. The distinguishing feature of an integrally stiffened composite is that the stiffening system has been manufactured simultaneously as part of the stiffened composite structure.

*This paper is declared a work of the U.S. Government and is not subject to copyright protection in the United States

Paper presented at the RTO AVT Specialists' Meeting on "Application of Damage Tolerance Principles for Improved Airworthiness of Rotorcraft", held in Corfu, Greece, 21-22 April 1999, and published in RTO MP-24.

Critical components of a structure are required to remain safe and be able to function under loading after experiencing some damage. The cause of damage may be an accident, defect, or unexpected overloading. Damage tolerance of a structure is quantified by the residual strength, that is the additional load carrying ability after damage. Composite structures are well suited for design with emphasis on damage tolerance as continuous fiber composites have the ability to arrest cracks and prevent self-similar crack propagation. It is difficult to design and certify a composite structure because of the complexities in predicting the overall congruity and performance of fiber composites under various loading and hygrothermal conditions.

Design considerations with regard to the durability of fiber composite structures require an a priori evaluation of damage initiation and fracture propagation mechanisms under expected loading and service environments. Concerns for safety and survivability of critical components require a quantification of the structural fracture resistance under loading. A significant design parameter with regard to composite damage tolerance is the laminate configuration. In general, quasiisotropic laminates yield better damage tolerance. However, in many cases a quasiisotropic laminate may not be the most efficient with regard to structural strength and performance when there is no damage. For a rational design process it is necessary to quantify the structural damage tolerance for a candidate design. The ability of designing composites with numerous possible fiber orientation patterns, choices of constituent material combinations, ply drops and hybridizations, render a large number of possible design parameters that may be varied for an optimal design. Damage initiation and progression characteristics are much more complex for integrally stiffened fiber composites compared to homogenous or orthotropic materials. The structural fracture process of a fiber composite depends on many parameters such as laminate configuration, fiber volume ratio, constituent stiffness/strength/hygrothermal parameters, stiffening system, and the fabrication process. Recent developments in computational simulation technology have made it possible to evaluate the details of progressive damage and fracture in composite structures. Computational simulation enables assessment of the damage initiation and propagation loads. A damage energy release rate is evaluated globally during simulation by computing the work done per unit damage created. The damage energy release rate is used to quantify the structural damage tolerance at different stages of degradation. The influence of local defects or flaws and effects of the fabrication process in terms of residual stresses are taken into account.

An important feature of computational simulation is the assessment of damage stability or damage tolerance of a structure under loading. At any stage of damage progression, if there is a high level of structural resistance to damage progression under the service loading, the structure is stable with regard to fracture. The corresponding state of structural damage is referred to as *stable damage*. On the other hand, if damage progression does not encounter significant structural resistance, it corresponds to an *unstable damage* state. Unstable damage progression is characterized by very large increases in the amount of damage due to small increases in loading. Whereas during stable damage progression the amount of increase in damage is consistent with the increase in loading.

Internal damage in composites is often initiated as cracking due to normal stresses transverse to fiber orientation. At the presence of stress concentrations or defects, initial damage may also include fiber fracture. Further degradation is in the form of additional fiber fractures that usually lead to structural fracture. Because of the numerous possibilities with material combinations, composite geometry, fiber orientations, and loading conditions, it is essential to have an effective computational capability to predict the behavior of composite structures for any loading, geometry, composite material combinations, and boundary conditions. The predictions of damage initiation, growth, accumulation, and propagation to fracture are important in evaluating the load carrying capacity and reliability of composite structures. Quantification of the structural fracture resistance is also required to evaluate the durability/life of composite structures.

Laminated composite design practice has been based on extensive testing with attempts to apply formal fracture mechanics concepts to interpret test results. In certain cases interpretation of laminated composite test data via fracture mechanics has been satisfactory. However, in most cases fracture mechanics methods have significantly mispredicted the strength of fiber composites. Reconciliation of test results with fracture mechanics has required significant modifications of effective fracture toughness and specific, laminate configuration dependent, effective stress concentration field parameters. Additionally, required adjustments of fracture mechanics parameters have had to be reassessed with every change in constituent and laminate characteristics. The complete evaluation of laminated composite fracture requires an assesment of ply and subply

level damage/fracture processes.

Continuous fiber composites in general have the ability to arrest cracks and prevent self-similar crack propagation. For most fiber reinforcement configurations, cracks and other stress concentrators do not have as important an influence in composites as they do for homogeneous materials. Another important aspect is the multiplicity of design options for composites. The ability of designing composites with numerous possible fiber orientation patterns, choices of constituent material combinations, ply drops, hybridizations, and integrated stiffening options render a large number of possible design parameters that may be varied for an optimal design.

The present approach by-passes traditional fracture mechanics to provide an alternative evaluation method, conveying to the design engineer a detailed description of damage initiation, growth, accumulation, and propagation that would take place in the process of ultimate fracture of an integrally stiffened fiber composite structure. Results show in detail the damage progression sequence and structural fracture resistance during different degradation stages. This paper demonstrates that computational simulation, with the use of established material modeling and finite element modules, adequately tracks the damage growth and subsequent propagation to fracture for an integrally stiffened fiber composite structure.

METHODOLOGY

Computational simulation is implemented via the integration of three modules: (1) composite mechanics, (2) finite element analysis, and (3) damage progression tracking. The overall evaluation of composite structural durability is carried out in the damage progression module (Minnetyan et al 1990) that keeps track of composite degradation for the entire structure. The damage progression module relies on the composite mechanics code (Murthy and Chamis 1986) for composite micromechanics, macromechanics and laminate analysis, and calls a finite element analysis module that uses anisotropic thick shell elements to model laminated composites (Nakazawa et al 1987).

A computational simulation cycle begins with the definition of constituent properties from a materials databank. Composite ply properties are computed by the composite mechanics module. The composite mechanics module also computes through-the-thickness structural properties of each laminate. The finite element analysis module accepts the composite properties that are computed by the composite mechanics module at each node and performs the analysis for a load increment. After an incremental finite element analysis, the computed generalized nodal force resultants and deformations are supplied to the composite mechanics module that evaluates the nature and amount of local damage, if any, in the plies of the composite laminate. Individual ply failure modes are determined using failure criteria associated with the negative and positive limits of the six ply-stress components ($\sigma_{\ell 11}$, $\sigma_{\ell 22}$, $\sigma_{\ell 33}$, $\sigma_{\ell 12}$, $\sigma_{\ell 13}$, $\sigma_{\ell 23}$), a modified distortion energy (MDE) combined stress failure criterion. The MDE failure criterion is expressed as:

$$F = 1 - \left(\frac{\sigma_{\ell 11\alpha}}{S_{\ell 11\alpha}}\right)^2 - \left(\frac{\sigma_{\ell 22\beta}}{S_{\ell 22\beta}}\right)^2 + K_{\ell 12\alpha\beta}\frac{\sigma_{\ell 11\alpha}}{S_{\ell 11\alpha}}\frac{\sigma_{\ell 22}}{S_{\ell 22}} - \left(\frac{\sigma_{\ell 12S}}{S_{\ell 12S}}\right)^2 \quad (1)$$

where α and β indicate tensile or compressive stress, $S_{\ell 11\alpha}$ is the local longitudinal strength in tension or compression, $S_{\ell 22\alpha}$ is the transverse strength in tension or compression, and

$$K_{\ell 12\alpha\beta} = \frac{(1+4\nu_{\ell 12}-\nu_{\ell 13})E_{\ell 22}+(1-\nu_{\ell 23})E_{\ell 11}}{[E_{\ell 11}E_{\ell 22}(2+\nu_{\ell 12}+\nu_{\ell 13})(2+\nu_{\ell 21}+\nu_{\ell 23})]^{1/2}} \quad (2)$$

The type of failure is assessed by comparison of the magnitudes of the squared terms in Equation (1). Depending on the dominant term in the MDE failure criterion, fiber failure or matrix failure is assigned.

The generalized stress-strain relationships for each node are revised according to the composite damage evaluated by the composite mechanics module after each finite element analysis. The model is automatically updated with a new finite element mesh and properties, and the structure is reanalyzed for further deformation and damage. If ply failure criteria indicate new or additional damage during a load increment, the damage tracking module degrades the composite properties affected by the damage and reanalizes the structure under the same load. When there is no indication of further damage under a load, the structure is considered to be in equilibrium. Subsequently, another load increment is applied leading to possible damage growth, accumulation, or propagation. In the computational simulation cases presented in this paper, analysis is stopped when commencement of the damage propagation phase is indicated by laminate fracture. Laminate fracture is predicted when major principal failure criteria are met for all plies

at a node. After laminate fracturing, the composite structure is anticipated to enter a final damage propagation stage that leads to ultimate structural fracture or collapse.

During progressive damage tracking the following terminology is utilized to describe the various stages of degradation in the composite structure: (1) *damage initiation* refers to the start of damage induced by loading that the composite structure is designed to carry; (2) *damage growth* is the progression of damage from the location of damage initiation to other regions; (3) *damage accumulation* is the increase in the amount of damage in the damaged regions with additional damage modes becoming active; (4) *damage propagation* is the rapid progression of damage to other regions of the structure; (5) *structural fracture* is the ultimate disintegration of the specimen.

INTEGRALLY STIFFENED PANEL

A graphite/epoxy laminated composite plate with integrated ±45° intermittent lattice stiffeners was investigated with damage and fracture propagation due to tension, compression, and in-plane shear loads. The response of the integrally stiffened composite panel was compared with that of an unstiffened skin plate. The unstiffened plate was given additional skin thickness such that the material volume was the same as the material volume of the integrally stiffened plate. The additional plies of the unstiffened plate were given fiber orientations of ±45°, same as the fiber orientations of the integrated stiffeners. Both the unstiffened and integrally stiffened panels were made of AS-4 graphite fibers in a high modulus high strength epoxy matrix (AS-4/HMHS). Ply layup of the unstiffened panel was $[\pm 45/0/90/\pm 45]_S$. The stiffened panel had a skin layup of $[0/90/\pm 45]_S$. The stiffener plies were added to the top of the skin as $[+45]_8$ or as $[-45]_8$. Ply thickness was 0.127 mm (0.005 in). The fiber volume ratio was V_f=0.60 and the void volume ratio vas V_v=0.01. The cure temperature was T_{cu}=177°C (350°F). The fiber and matrix properties were obtained from a databank of composite constituent material properties resident in the composite mechanics module (Murthy and Chamis 1986). The fiber and matrix properties corresponding to this case are given in Tables I and II, respectively. The HMHS matrix properties are representative of the 3501-6 resin. These in-situ properties are similar to those identified by Sobel et al (1993) with experimental correlation.

The panels had identical planar geometry with a width of 305 mm (12.0 in.) and length of 457 mm (18 in.). Each finite element model contained 117 nodes and 96 uniformly sized square elements. Figure 2 shows the finite element model with diagonal lines along the ±45° stiffener bands. Numbers at nodes indicate the laminate type number at that node for the integrally stiffened panel. Laminate type 1 had a layup of $[0/90/\pm 45]_S$, representing the skin. Laminate type 2 had the skin layup plus $[+45]_8$ representing the +45 stiffened nodes. Laminate type 3 had the skin layup plus $[-45]_8$ representing the -45 stiffened nodes. Laminate type 4 had the skin layup plus $[+45_8/-45_8]$ representing intersection nodes for +45 and -45 stiffeners. Panels were assumed to be simply supported for structural response; i.e. the left end nodes of the panel were restrained against all displacement components and the right end nodes were restrained against displacement normal to the plane of the panel. Additionally, the right end nodes were constrained to have uniform displacement in the plane of the panel via duplicate node specifications.

Structural response characteristics of the integrally stiffened panel were evaluated in terms of the buckling load and the bending stiffness. Analysis of the integrally stiffened panel under uniaxial compression indicated a buckling load of 1,114 N (250 lbs). The buckling load of the unstiffened panel was only 213 N (48 lbs). Therefore the buckling resistance of the integrally stiffened panel was 5.2 times that of the unstiffened panel with the same amount of composite material. Similarly, the bending rigidity was significantly improved due to integrated stiffeners. Figure 3 shows a comparison of the midspan deflections of unstiffened and integrally stiffened panels due to uniform bending moment applied to the simply supported right end of the panel. Figure 3 shows that the integrally stiffened panel was 7.2 times stiffer than the unstiffened panel in bending.

Next, the in-plane progressive damage and fracture responses were compared for the unstiffened and stiffened panels. Figure 4 shows damage progressions of unstiffened and integrally stiffened panels subjected to tension. Damage initiation for the integrally stiffened panel occurred in the 90° skin plies due to transverse tensile fractures. Damage initiation for the unstiffened panels was also in the 90° plies due to transverse tensile fractures. In both cases the MDE combined stress failure criterion was activated. However, the damage initiation load for the integrally stiffened panel was approximately one third of the damage initiation load for the flat panel with the same material volume. Figure 5 shows the

displacements in tension. The uniaxial stiffnesses of the unstiffened and integrally stiffened panels are approximately the same prior to damage initiation. However, stiffness of the integrally stiffened panel degrades quickly due to damage initiation and progression. Figure 6 shows damage progressions of the unstiffened and integrally stiffened panels under uniaxial compression. Damage initiation for the integrally stiffened panel occurred at the edge of the panel at midspan where +45 and -45 stiffeners converged (laminate type 4). The damage initiation modes included the transverse tensile and longitudinal compressive failures of the 90° skin plies, in-plane shear failures of the ±45° skin plies, as well as the in-plane shear failures of the +45 stiffener plies near the skin. Damage initiation for the unstiffened panels under compression was in the 0° plies due to longitudinal compressive fractures. The damage propagation load of the unstiffened panel was more than five times that of the integrally stiffened panel. The initial stiffnesses of the unstiffened and integrally stiffened panels in compression were the same as observable from Figure 7. However, the stiffness of the integrally stiffened panel degraded at a much lower loading compared to degradation load of the flat panel. Figure 8 shows the damage progressions of unstiffened and integrally stiffened panels under in-plane simple shear loading. Damage initiation for the integrally stiffened panel was due to longitudinal compressive failure of a +45 skin ply at a type 3 stiffened node. On the other hand, damage initiation for the flat panel under shear was due to transverse tensile failures of the 90° plies. As it was in tension and compression, also in shear the integrally stiffened panel degraded at a lower load compared to the flat panel. Figure 9 shows the load-displacement relationships in shear. Computational simulation results depicted in Figure 9 indicate that in shear, the initial stiffness of the flat panel was slightly higher than that of the integrally stiffened panel.

INTEGRALLY STIFFENED COMPOSITE SHELL

A composite cylindrical shell with and without integrated ±45° intermittent lattice stiffeners was investigated with damage and fracture propagation due to axial tension, as well as internal and external pressure loads. The response of the integrally stiffened shell was compared with that of an unstiffened shell. The unstiffened shell was given additional skin thickness such that the material volume was the same as the material volume of the integrally stiffened shell. The additional plies of the unstiffened shell were given fiber orientations of ±45°, same as the fiber orientations of the integrated stiffeners. Both the unstiffened and integrally stiffened shells were made of AS-4/HMHS composite. Ply layup of the unstiffened shell was $[\pm 45/0/90/\pm 45]_S$. The stiffened shell had a skin layup of $[0/90/\pm 45]_S$. The stiffener plies were added to the top of the skin as $[+45]_8$ or as $[-45]_8$. Ply thickness was 0.127 mm (0.005 in). The fiber volume ratio was V_f=0.60 and the void volume ratio vas V_v=0.01. The cure temperature was T_{cu}=177°C (350°F).

Each cylindrical shell finite element model contained 400 nodes and 384 uniformly sized square elements. Figure 10 shows the finite element model for a cylindrical shell. The shell was simulated subject to increasing levels of internal and external pressurizations as well as axial loading. To represent the axial stresses produced in the closed end pressure vessel, boundary nodes at one end of the cylinder were subjected to force resultants in the axial direction, whereas the boundary FEM nodes were restrained in the axial direction at the opposite end. The uniformly distributed axial tension was such that the generalized axial stresses in the shell wall were half those developed in the hoop direction.

Figure 11 shows a comparison of damage progressions for the integrally stiffened and unstiffened composite shells under axial tension. Figure 11 indicates that ultimate strength of the integrally stiffened cylindrical shell is approximately 60 percent of the ultimate strength of shell without integral stiffeners. Additionally, damage initiation for the integrally stiffened shell begins at only 10 percent of the ultimate load. On the other hand, damage initiation for the unstiffened shell corresponds to a loading level that is approximately 97 percent of its ultimate load. Figure 12 shows the exhausted cumulative damage energy based on depleted energies of the local failure modes. The exhausted damage energy represents a similar pattern of damage progression as the percent damage volume depicted in Figure 12. Figure 13 shows the damage energy release rates (DERR) based on the incremental work done by applied loading during damage progression of the integrally stiffened cylindrical shell. Peak values in the DERR levels indicate significant damage events. The first peak in DERR corresponding to damage initiation for the integrally stiffened shell occurred due to transverse tensile fractures in the 90° skin plies. The steep increase in DERR at approximately 11 kN (2.5 k) axial tension corresponds to a partial separation between skin and

stiffener plies.

Figure 14 shows comparison of damage progressions for integrally stiffened and unstiffened cylindrical shells subjected to external pressures. The ultimate pressure for the integrally stiffened shell is approximately 75 percent of the ultimate pressure for the unstiffened shell. Damage initiation for the integrally stiffened shell occurs at 23 percent of its ultimate pressure. On the other hand damage initiation for the unstiffened shell occurs at approximately 94 percent of its ultimate pressure. Also, the volume of damage in the integrally stiffened shell at ultimate pressure is much greater than the volume of damage in the unstiffened shell at ultimate pressure.

SUMMARY OF RESULTS

This section summarizes some of the insights gained by the present investigation as applicable to graphite/epoxy laminated composite structures with integrated stiffeners, as follows:

1. Integrated stiffeners may be used to increase the out-of-plane stiffness properties significantly.
2. The improvement of out of plane stiffness is paid for by the degradation of in-plane damage tolerance and durability characteristics.
3. Damage initiation occurred much sooner for the integrally stiffened composite structures subjected to in-plane tension, compression, or shear.
4. Damage initiation occurred in the skin plies for all cases considered.
5. For the integrally stiffened composites, damage initiation was within the skin at stiffened nodes.

GENERALIZATION OF PROCEDURE

The present computational simulation method is suitable for the design and continued in-service evaluation of composite structures. Composite structures with different constituents and ply layups can be evaluated under any loading.

Structural health monitoring is based on damage tolerance requirements defined via the computational simulation method. A damage tolerance parameter is described as the state of damage after the application of a given load level, normalized with respect to the damage state corresponding to ultimate fracture. Identification of damage progression mechanisms and the sequence of progressive fracture modes conveys useful information to evaluate structural safety. Computational simulation results can be formulated into health monitoring criteria, increasing the reliability of composite structures. The simulated failure modes and the type of failure provide the necessary quantitative and qualitative information to design an effective health monitoring system. Computed local damage energy release rates are correlated with the magnitudes of acoustic emission signals and other damage monitoring means such as piezoelectric stress sensors and strain gages that are an integral part of a composite structure. Fiber optics data networks embedded in the composite structure would transmit the detected local damage information to an expert system that provides feedback and reduces power to delay failure.

The basic procedure is to simulate a computational model of the composite structure subjected to the expected loading environments. Various fabrication defects and accidental damage may be represented at the ply and constituent levels, as well as at the laminate level. Computational simulation may be used to address various design and health monitoring questions as follows:

1. Evaluation of damage tolerance: Computational simulation will generate the damage that would be caused due to overloading by the type of load the structure is designed to carry. On the other hand, a fabrication defect or accidental damage produced by inadvertent loading that is not an expected service load can be included in the initial computational model. Once the composite damage is defined, damage tolerance can be evaluated by monitoring damage growth and progression from the damaged state to ultimate fracture. Significant parameters that quantify damage stability and fracture progression characteristics are the rate of damage increase with incremental loading, and the changes in the structural response characteristics with loading. Identification of damage initiation/progression mechanisms and the sequence of progressive fracture modes convey serviceable information to help with critical decisions in the structural design and health monitoring process. Determination of design allowables based on damage tolerance requirements is an inherent use of the computational simulation results. Simulation of progressive fracture from defects allows setting of qual-

ity acceptance criteria for composite structures as appropriate for each functional requirement. Detailed information on specific damage tolerance characteristics help establish criteria for the retirement of a composite structure from service for due cause.

2. Determination of sensitive parameters affecting structural fracture: Computational simulation indicates the damage initiation, growth, and progression modes in terms of a damage index that is printed out for the degraded plies at each damaged node. In turn, the damage index points out the fundamental physical parameters that characterize the composite degradation. For instance, if the damage index shows ply transverse tensile failure, the fundamental physical parameters are matrix tensile strength, fiber volume ratio, matrix modulus, and fiber transverse modulus; of which the most significant parameter is the matrix tensile strength (Murthy and Chamis, 1986). In addition to the significant parameters pointed out by the ply damage index, sensitivity to hygrothermal parameters may be obtained by simulating the composite structure at different temperatures and moisture contents. Similarly, sensitivity to residual stresses may be assessed by simulating the composite structure fabricated at different cure temperatures. Identification of the important parameters that significantly affect structural performance for each design case allows optimization of the composite for best structural performance. Sensitive parameters may be constituent strength, stiffness, laminate configuration, fabrication process, and environmental factors.

3. Interpretation of experimental results for design decisions: Computational simulation allows interactive experimental-numerical assessment of composite structural performance. Simulation can be used prior to testing to identify locations and modes of composite damage that need be monitored by proper instrumentation and inspection of the composite structure. Interpretation of experimental data can be significantly facilitated by detailed information from computational simulation. Subscale experimental results may be extended to full prototype structures without concern for scale effects since computational simulation does not presume any global parameters but is based on constituent level damage tracking.

CONCLUSIONS

On the basis of the results obtained from the investigated flat composite plate, integrally stiffened panel, integrally stiffened and unstiffened composite cylindrical shell examples and from the general perspective of the available computational simulation method, the following conclusions are drawn:

1. Computational simulation can be used to track the details of damage initiation, growth, and subsequent propagation to fracture for unstiffened and integrally stiffened composite structures.
2. For the considered integral stiffening system, out-of-plane structural response characteristics such as the buckling load and the bending stiffness are significantly improved.
3. In-plane load carrying capability of a composite panel is reduced due to damage initiation and progression processes caused by the presence of integrated stiffeners.
4. Computational simulation, with the use of established composite mechanics and finite element modules, can be used to predict the influence of composite geometry as well as loading and material properties on the durability of composite structures.
5. The demonstrated procedure is flexible and applicable to all types of constituent materials, structural geometry, and loading. Hybrid composites and homogeneous materials, as well as laminated, stitched, woven, and braided composites can be simulated.
6. Computational simulation by CODSTRAN represents a new global approach to progressive damage and fracture assessment for any structure.

REFERENCES

1. C. C. Chamis and G. T. Smith, "Composite Durability Structural Analysis," NASA TM–79070, 1978.

2. T. B. Irvine and C. A. Ginty, "Progressive Fracture of Fiber Composites," *Journal of Composite Materials*, Vol. 20, March 1986, pp. 166-184.

3. L. Minnetyan, C. C. Chamis, and P. L. N. Murthy, "Structural Behavior of Composites with Progressive Fracture," *Journal of Reinforced Plastics and Composites*, Vol. 11, No. 4, April 1992, pp. 413-442

4. L. Minnetyan, P. L. N. Murthy, and C. C. Chamis, "Progression of Damage and Fracture in Composites under Dynamic Loading," NASA TM–103118, April 1990, 16 pp.

5. L. Minnetyan, P. L. N. Murthy, and C. C. Chamis, "Composite Structure Global Fracture Toughness via Computational Simulation," *Computers & Structures*, Vol. 37, No. 2, pp.175-180, 1990

6. L. Minnetyan, P. L. N. Murthy, and C. C. Chamis, "Progressive Fracture in Composites Subjected to Hygrothermal Environment," *International Journal of Damage Mechanics*, Vol. 1, No. 1, January 1992, pp. 60-79

7. L. Minnetyan, C. C. Chamis, and P. L. N. Murthy, "Damage and Fracture in Composite Thin Shells," NASA TM–105289, November 1991

8. C. C. Chamis, P. L. N. Murthy, and L. Minnetyan, "Progressive Fracture of Polymer Matrix Composite Structures: A New Approach," NASA TM–105574, January 1992, 22 pp.

9. L. Minnetyan, J. M. Rivers, P. L. N. Murthy, and C. C. Chamis, "Structural Durability of Stiffened Composite Shells," Proceedings of the 33rd SDM Conference, Dallas, Texas, April 13-15, 1992, Vol. 5, pp. 2879-2886

10. L. Minnetyan and P. L. N. Murthy,"Design for Progressive Fracture in Composite Shell Structures," Proceedings of the 24th International SAMPE Technical Conference, Toronto, Canada, October 20-22, 1992, pp. T227-T240

11. P. L. N. Murthy and C. C. Chamis, *Integrated Composite Analyzer (ICAN): Users and Programmers Manual*, NASA Technical Paper 2515, March 1986.

12. S. Nakazawa, J. B. Dias, and M. S. Spiegel, *MHOST Users' Manual*, Prepared for NASA Lewis Research Center by MARC Analysis Research Corp., April 1987.

13. L. Sobel, C. Buttitta, and J. Suarez, "Probabilistic & Structural Reliability Analysis of Laminated Composite Structures Based on IPACS Code," Proceedings of the 34th SDM Conference, LaJolla, California, April 19-22, 1993, Vol. 2, pp. 1207-1217

TABLE I: AS-4 Fiber Properties:

Number of fibers per end = 10000
Fiber diameter = 0.00762 mm (0.300E-3 in)
Fiber Density = 4.04E-7 Kg/m^3 (0.063 lb/in^3)
Longitudinal normal modulus = 200 GPa (29.0E+6 psi)
Transverse normal modulus = 13.7 GPa (1.99E+6 psi)
Poisson's ratio (ν_{12}) = 0.20
Poisson's ratio (ν_{23}) = 0.25
Shear modulus (G_{12}) = 13.8 GPa (2.00E+6 psi)
Shear modulus (G_{23}) = 6.90 GPa (1.00E+6 psi)
Longitudinal thermal expansion coefficient = -1.0E-6/°C (-0.55E-6 /°F)
Transverse thermal expansion coefficient = 1.0E-5/°C (0.56E-5 /°F)
Longitudinal heat conductivity = 301 kJ-m/hr/m^2/°C (4.03 BTU-in/hr/in^2/°F)
Transverse heat conductivity = 30.1 kJ-m/hr/m^2/°C (.403 BTU-in/hr/in^2/°F)
Heat capacity = 0.712 kJ/kg/°C (0.17 BTU/lb/°F)
Tensile strength = 3.09 GPa (448 ksi)
Compressive strength = 3.09 GPa (448 ksi)

TABLE II: HMHS Matrix Properties:

Matrix density = 3.40E-7 Kg/m^3 (0.0457 lb/in^3)
Normal modulus = 4.14 GPa (600 ksi)
Poisson's ratio = 0.34
Coefficient of thermal expansion = 0.72E-4/°C (0.40E-4 /°F)
Heat conductivity = 0.648 kJ-m/hr/m^2/°C (0.868E-2 BTU-in/hr/in^2/°F)
Heat capacity = 1.047 KJ/Kg/°C (0.25 BTU/lb/°F)
Tensile strength = 71.0 MPa (10.3 ksi)
Compressive strength = 423 MPa (61.3 ksi)
Shear strength = 161 MPa (23.4 ksi)
Allowable tensile strain = 0.02
Allowable compressive strain = 0.05
Allowable shear strain = 0.04
Allowable torsional strain = 0.04
Void conductivity = 16.8 J-m/hr/m^2/°C (0.225 BTU-in/hr/in^2/°F)
Glass transition temperature = 216°C (420°F)

LIST OF FIGURE CAPTIONS

Figure 1 Computational Simulation Cycle

Figure 2 Finite Element Model with Square Elements
Diagonal Lines are along the Integrated Stiffeners; AS-4/HMHS$[0/90/\pm45]_S$
Width = 305 mm; Length = 457 mm

Figure 3 Deflections of Panels due to Bending
Graphite-epoxy: AS-4/HMHS$[0/90/\pm45]_S$
Solid line: flat panel
Dashed line: integrally stiffened panel

Figure 4 Damage Progression under Uniaxial Tension
Graphite-epoxy: AS-4/HMHS$[0/90/\pm45]_S$
Solid line: flat panel
Dashed line: integrally stiffened panel

Figure 5 Displacements under Uniaxial Tension
Graphite-epoxy: AS-4/HMHS$[0/90/\pm45]_S$
Solid line: flat panel
Dashed line: integrally stiffened panel

Figure 6 Damage Progression under Compression
Graphite-epoxy: AS-4/HMHS$[0/90/\pm45]_S$
Solid line: flat panel
Dashed line: integrally stiffened panel

Figure 7 Displacements under Uniaxial Compression
Graphite-epoxy: AS-4/HMHS$[0/90/\pm45]_S$
Solid line: flat panel
Dashed line: integrally stiffened panel

Figure 8 Damage Progression under In-plane Shear
Graphite-epoxy: AS-4/HMHS$[0/90/\pm45]_S$
Solid line: flat panel
Dashed line: integrally stiffened panel

Figure 9 Displacements under In-plane Simple Shear
Graphite-epoxy: AS-4/HMHS$[0/90/\pm45]_S$
Solid line: flat panel
Dashed line: integrally stiffened panel

Figure 10 Finite Element Model of Cylindrical Shell
AS-4/HMHS$[0/90/\pm45]_S$

Figure 11 Damage Progression under Axial Tension
Graphite-epoxy: AS-4/HMHS$[0/90/\pm45]_S$
Solid line: unstiffened shell
Dashed line: integrally stiffened shell

Figure 12 Exhusted Damage Energy under Tension
Graphite-epoxy: AS-4/HMHS$[0/90/\pm45]_S$
Solid line: unstiffened shell
Dashed line: integrally stiffened shell

Figure 13 Damage Energy Release Rates under Tension
Graphite-epoxy: AS-4/HMHS$[0/90/\pm45]_S$
Solid line: unstiffened shell
Dashed line: integrally stiffened shell

Figure 14 Damage Progression under External Pressure
Graphite-epoxy: AS-4/HMHS$[0/90/\pm45]_S$
Solid line: unstiffened shell
Dashed line: integrally stiffened shell

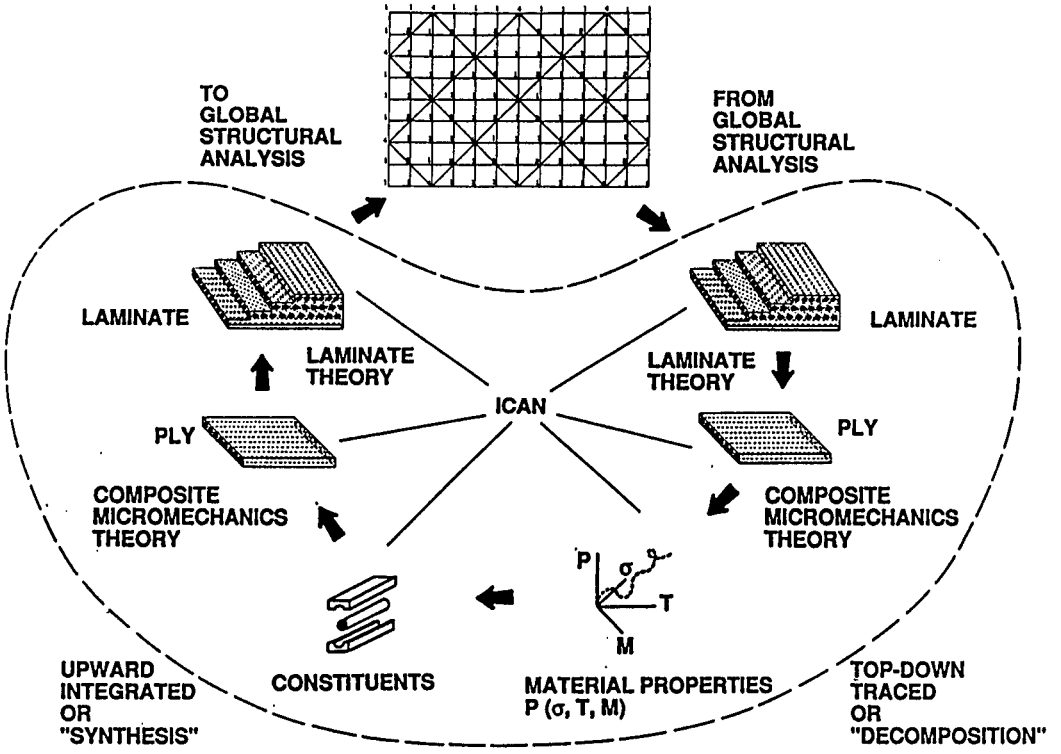

Figure 1 Computational Simulation Cycle

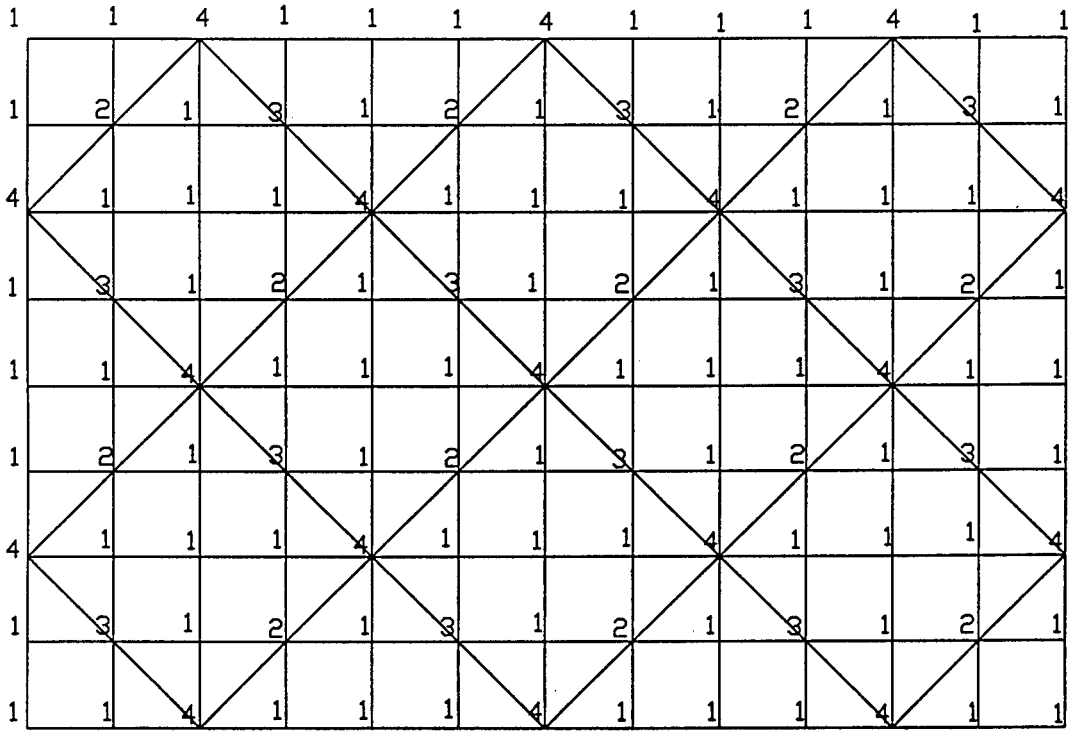

Figure 2 Finite Element Model with Square Elements
Diagonal Lines are along the Integrated Stiffeners
AS-4/HMHS$[0/90/\pm45]_S$; Width = 305 mm; Length = 457 mm

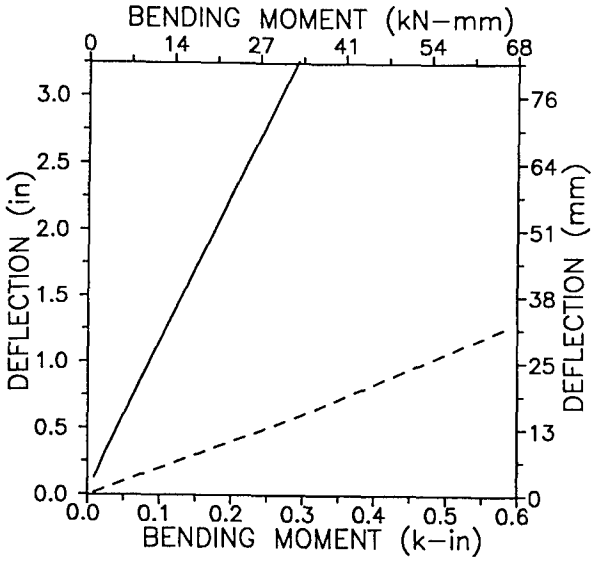

Figure 3 Deflections of Panels due to Bending
Graphite-epoxy: AS-4/HMHS$[0/90/\pm45]_S$
Solid line: flat panel
Dashed line: integrally stiffened panel

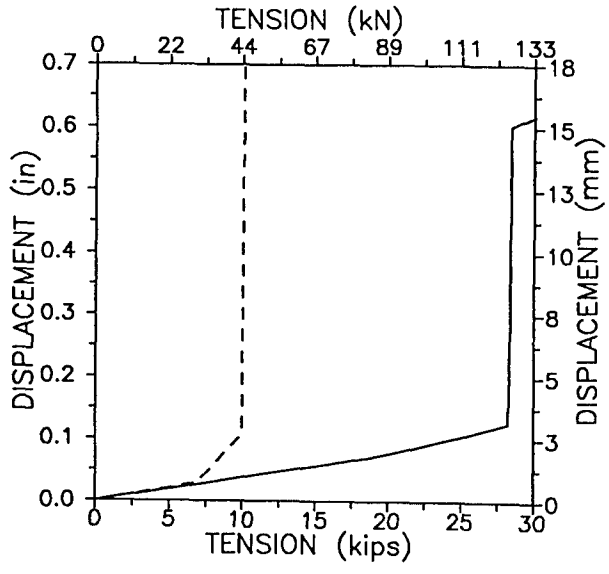

Figure 5 Displacements under Uniaxial Tension
Graphite-epoxy: AS-4/HMHS$[0/90/\pm45]_S$
Solid line: flat panel
Dashed line: integrally stiffened panel

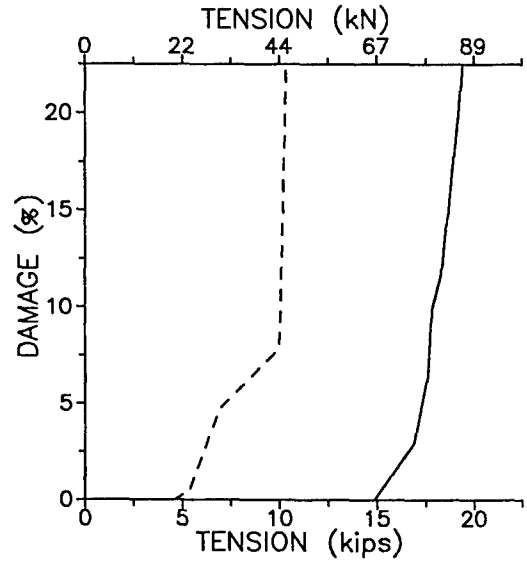

Figure 4 Damage Progression under Uniaxial Tension
Graphite-epoxy: AS-4/HMHS$[0/90/\pm45]_S$
Solid line: flat panel
Dashed line: integrally stiffened panel

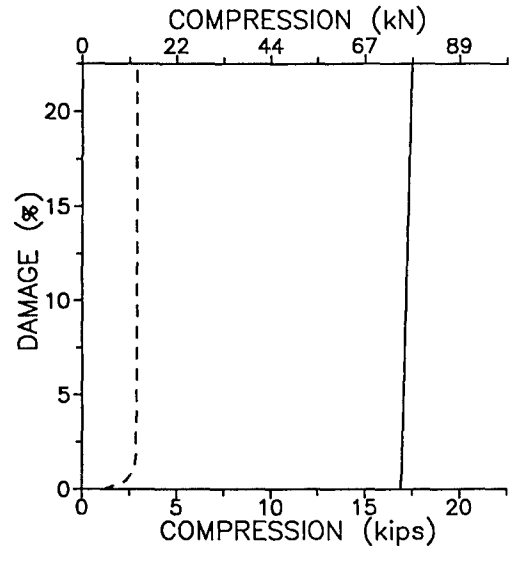

Figure 6 Damage Progression under Compression
Graphite-epoxy: AS-4/HMHS$[0/90/\pm45]_S$
Solid line: flat panel
Dashed line: integrally stiffened panel

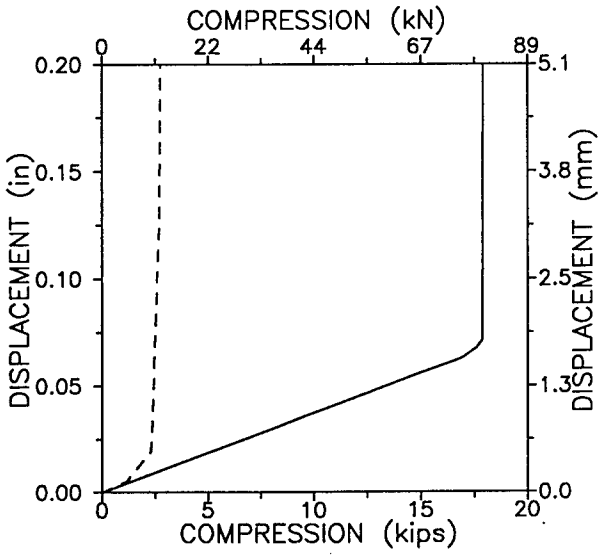

Figure 7 Displacements under Uniaxial Compression
Graphite-epoxy: AS-4/HMHS[0/90/±45]$_S$
Solid line: flat panel
Dashed line: integrally stiffened panel

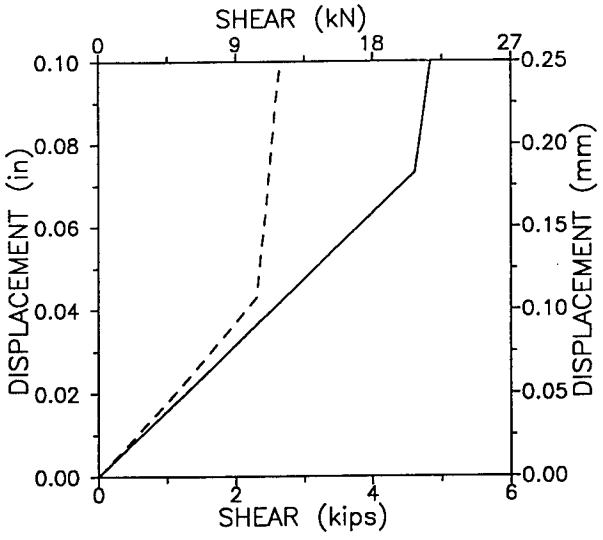

Figure 9 Displacements under In-plane Simple Shear
Graphite-epoxy: AS-4/HMHS[0/90/±45]$_S$
Solid line: flat panel
Dashed line: integrally stiffened panel

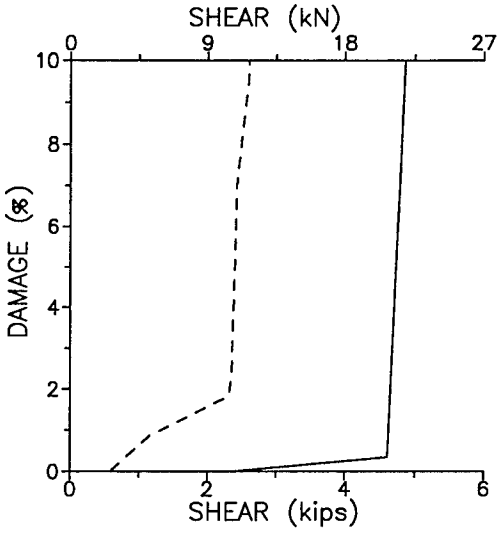

Figure 8 Damage Progression under In-plane Shear
Graphite-epoxy: AS-4/HMHS[0/90/±45]$_S$
Solid line: flat panel
Dashed line: integrally stiffened panel

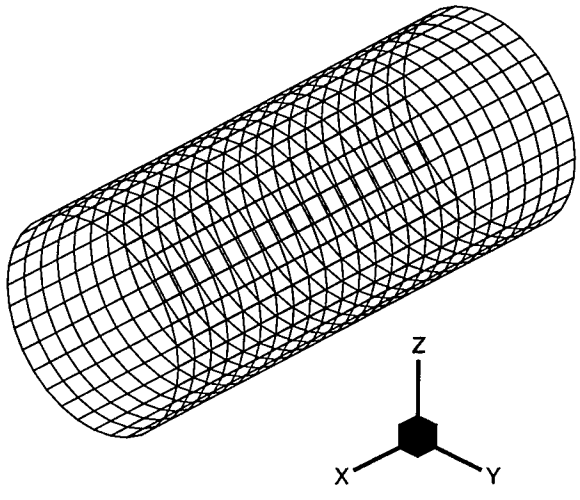

Figure 10 Finite Element Model of Cylindrical Shell
AS-4/HMHS[0/90/±45]$_S$

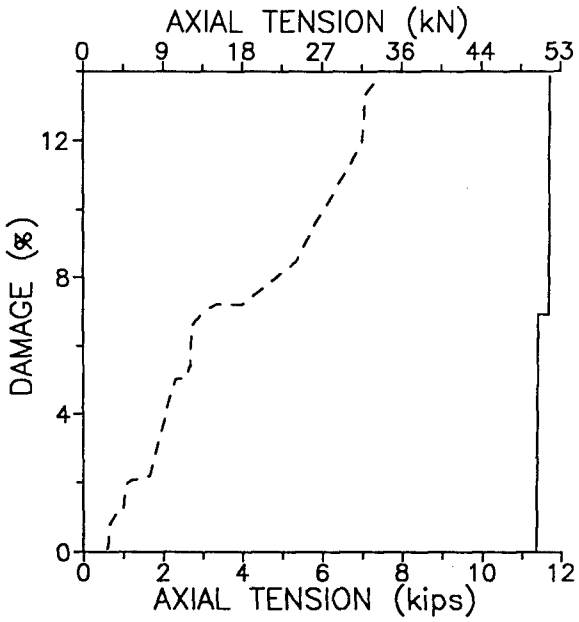

Figure 11 Damage Progression under Axial Tension
Graphite-epoxy: AS-4/HMHS[0/90/±45]$_S$
Solid line: unstiffened shell
Dashed line: integrally stiffened shell

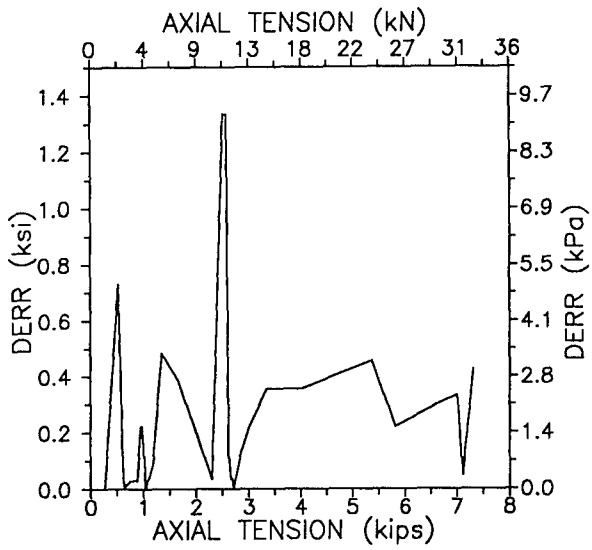

Figure 13 Damage Energy Release Rates under Tension
Graphite-epoxy: AS-4/HMHS[0/90/±45]$_S$
Solid line: unstiffened shell
Dashed line: integrally stiffened shell

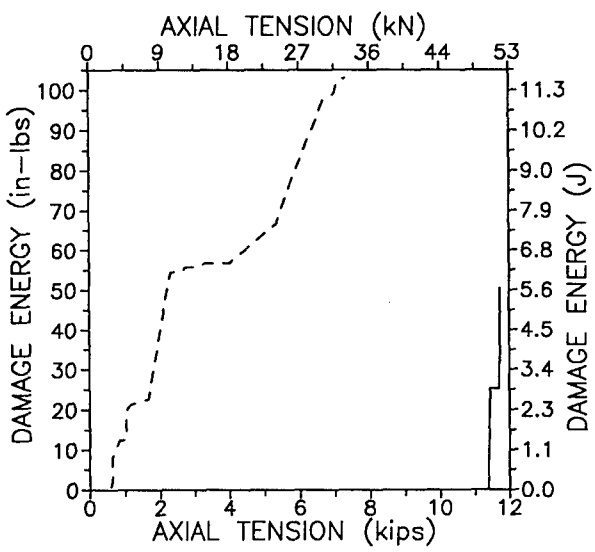

Figure 12 Exhusted Damage Energy under Tension
Graphite-epoxy: AS-4/HMHS[0/90/±45]$_S$
Solid line: unstiffened shell
Dashed line: integrally stiffened shell

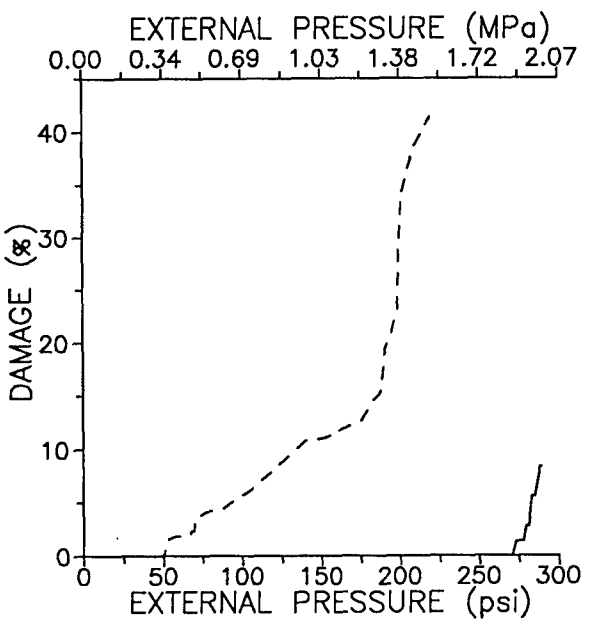

Figure 14 Damage Progression under External Pressure
Graphite-epoxy: AS-4/HMHS[0/90/±45]$_S$
Solid line: unstiffened shell
Dashed line: integrally stiffened shell